

Supporting information

Substituting copolymeric poly(alkylenetetrasulfide) for elemental sulfur to diminish the shuttling effect of modified intermediate polysulfides for high-performance lithium-sulfur batteries

He Zhou,¹ Faqi Yu,¹ Min Wei,¹ Yunlan Su,² Yuchen Ma,¹ Dujin wang,² Qiang Shen^{1*}

(Corresponding E-mail: qshen@sdu.edu.cn)

Experimental:

Materials and sample preparation

All the chemicals such as sublimed sulfur (S₈), dichloromethane (CH₂Cl₂) and dichloroethane (ClCH₂CH₂Cl) are of analytical grade and were used as purchased. Ultrapure water (18.2 MΩ·cm) was used throughout solution preparation.

Synthesis and characterization of serial copolymeric poly(alkylenetetrasulfide) with the formula of [(CH₂)_yS₄]_n (y = 1 or 2; n ~ the number of repeating units) have been well demonstrated in literatures.¹⁻⁴ At first, yellow-orange aqueous solution of sodium tetrasulfide (Na₂S₄) was obtained by the stoichiometric reaction of aqueous NaOH and molecular S₈, and then aqueous Na₂S₄ (50 mL) was transferred into a 100-mL three-necked round bottom flask equipped with a dropping funnel, condenser and thermometer. Subsequently, CH₂Cl₂ or ClCH₂CH₂Cl liquid (2 mL) was dropwise added into the aqueous Na₂S₄-containing flask at 40°C, and then a condensation polymerization reaction proceeded under vigorous stirring, shown as the following equation (1):



Finally, at a reaction interval of 2 h, a lumpy mass of linear copolymer poly(methylenetetrasulfide) or poly(ethylenetetrasulfide), abbreviated as PMTS or PETS, was taken out of the reaction system and was thoroughly washed with hot water.

Chitosan-derived porous carbon (CPC) was self-made in laboratory, and this guaranteed both the graphitization of framework CPC and its mainly microporous feature as demonstrated previously.^{5,6} The dispersion of a polymer PMTS/PETS in carbon disulfide (CS₂) or the solution of molecular S₈ in CS₂ was thoroughly soaked into CPC, resulting in a copolymer-containing or sulfur-encapsulated composite after the complete evaporation of the solvent. To assay the better cycling performance of a copolymer/CPC composite than that of composite S/CPC, the effective S-content in each composite was kept at a constant value of ~40 wt%.^{2,7-9}

Structural and electrochemical characterization

Fourier transform infrared spectroscopy (FT IR) data was obtained on a VERTEX-70 spectrometer using KBr tablet method. Nitrogen adsorption isotherms were measured on a micromeritics ASAP 2020 porosimeter at 77 K using a 10 s equilibrium interval. X-ray diffraction (XRD) patterns were recorded on a Rigaku D/max 2400 kV powder X-ray diffractometer with Cu K α radiation ($\lambda=1.5406 \text{ \AA}$, 40 kV, 120 mA) in the 2Theta range of 10 and 70°. Raman spectra were measured using a 632.8 nm laser with a LABRAM-HR confocal laser micro-Raman spectrometer. Thermogravimetric analysis (TGA) profiles were obtained on a Mettler Toledo TGA/SDTA851 machine with a heating rate of 10 °C min⁻¹ under N₂ atmosphere. Samples were dispersed in ethanol by ultrasonication and then deposited on a carbon film supported by copper grid, prior to transmission electron microscopy (TEM) and high-resolution TEM (HR TEM) measurements on a JEM 2100 microscope (200 kV). Scanning electron microscopy (SEM) was carried out with a JEOL JSM-6700F combined X-ray energy dispersive spectroscopy (EDS). X-ray photoelectron spectroscopy (XPS) analysis was performed on a VG Scientific ESCALAB 220i-XL electron spectrometer using Al K α radiation.

Cathode material (e.g., PMTS/CPC composite), acetylene black and sodium alginate binder were mixed in water at a mass ratio of 7.0:1.5:1.5, and the resulting slurry was pasted onto an aluminum foil and dried at 60°C for 12 h. And then, the aluminum foil was cut into discs (12 mm in diameter) and used as working electrodes with a mass loading of $1.4 \pm 0.4 \text{ mg cm}^{-2}$. Lithium foil, Celgard 2300 polymeric film and nickel foam were used as counter electrode, separator and current collector, respectively. An electrolyte solution (35 μL) of lithium bis(trifluoromethanesulfonyl)imide (LiTFSI, 1.0 M) and LiNO₃ (2.0 %) in the mixed solvent of 1,3-dioxanes and 1,2-dimethoxyethane (1:1, vol:vol)

was used to assemble 2032-type coin cells in an argon-filled glove box.

Galvanostatic cycling tests were conducted on a Land CT2001A battery system at 30°C between 1.8-2.7 V (*vs.* Li⁺/Li and hereafter). Cyclic voltammetry (CV) curves were recorded using an LK 2005A electrochemical workstation at 0.1 mV s⁻¹ within 1.5-3.0 V. Electrochemical impedance spectroscopy (EIS) data was obtained by an EG&G PAR 273A electrochemical workstation in the frequency range of 0.1 MHz - 0.01 Hz with an AC voltage amplitude of 5 mV.

Theoretical calculation

Theoretical calculations were performed using the Vienna Ab-initio Simulation Package (VASP) and the exchange-correlation term was the standard generalized gradient approximation (GGA) of Perdew-Burke-Ernzerhof (PBE) functionals.^{10,11} In view of the highly microporous nature of graphitized CPC framework, its single-layer graphene-like surface was defined as a polyaromatic hydrocarbon molecule containing 24 carbon atoms and 12 hydrogen atoms. The binding energy (E_b) between one lithium polysulfide (e.g., Li₂S_n, n = 4 or 6) and the graphene-like surface of graphitized CPC was estimated according to the expression of $E_b = E_{total} - (E_1 + E_2)$.

Wherein, E_1 , E_2 and E_{total} represent the energies of lithium polysulfide, single-layer graphene and their integrative configuration of Li₂S_n-CPC system, respectively. To simplify the calculation, van der Waals (vdW) interactions within density functional theory (DFT) were focused, and a plane-wave basis set at the kinetic energy cutoff of 400 eV was employed until the value of residual forces is smaller than 0.02 eV Å⁻¹.¹²

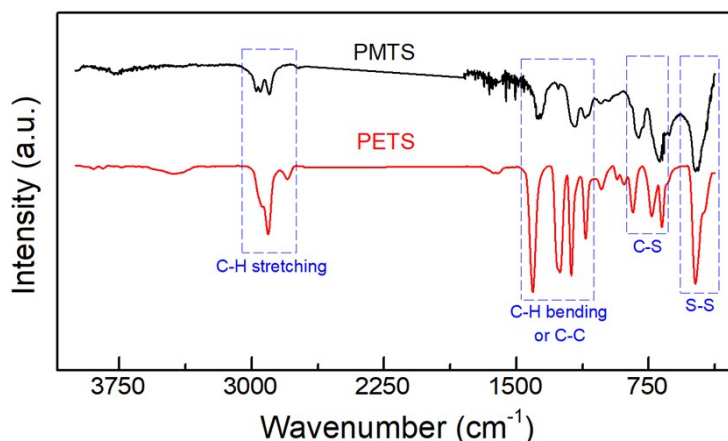


Fig. S1 FT IR spectra of as-synthesized PMTS and PETS copolymers, showing the characteristic absorptions of S-S (450-466 cm^{-1}), C-S (640-870 cm^{-1}), C-H bending (1050-1450 cm^{-1})

By comparison, along with the change of PMTS to PETS, the blue shift of C-H bending and the red shift of C-H stretching are observed, which may be attributed to the increasing number of methylene ($-\text{CH}_2-$) for the non-sulfur segments in these copolymeric backbones.

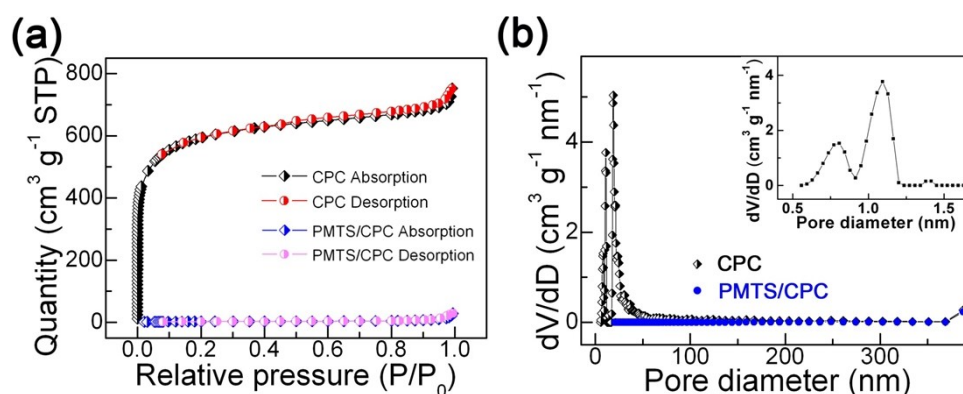


Fig. S2 (a) N_2 adsorption-desorption isotherms and (b) pore size distributions of pristine CPC and composite PMTS/CPC, and an inset in panel (d) presents the microspore size distribution of CPC.

Pristine porous carbon (CPC) has a high specific surface area of $2225.8 \text{ m}^2 \text{ g}^{-1}$ (the microporous fraction $\sim 1388.0 \text{ m}^2 \text{ g}^{-1}$) and a total pore volume of $1.16 \text{ cm}^3 \text{ g}^{-1}$ (the micropore size distribution, 0.5 - 1.2 nm; the microporous volume, $0.55 \text{ cm}^3 \text{ g}^{-1}$), and by comparison the specific surface area and average pore size of composite PMTS/CPC or PETS/CPC are too small to be omitted.

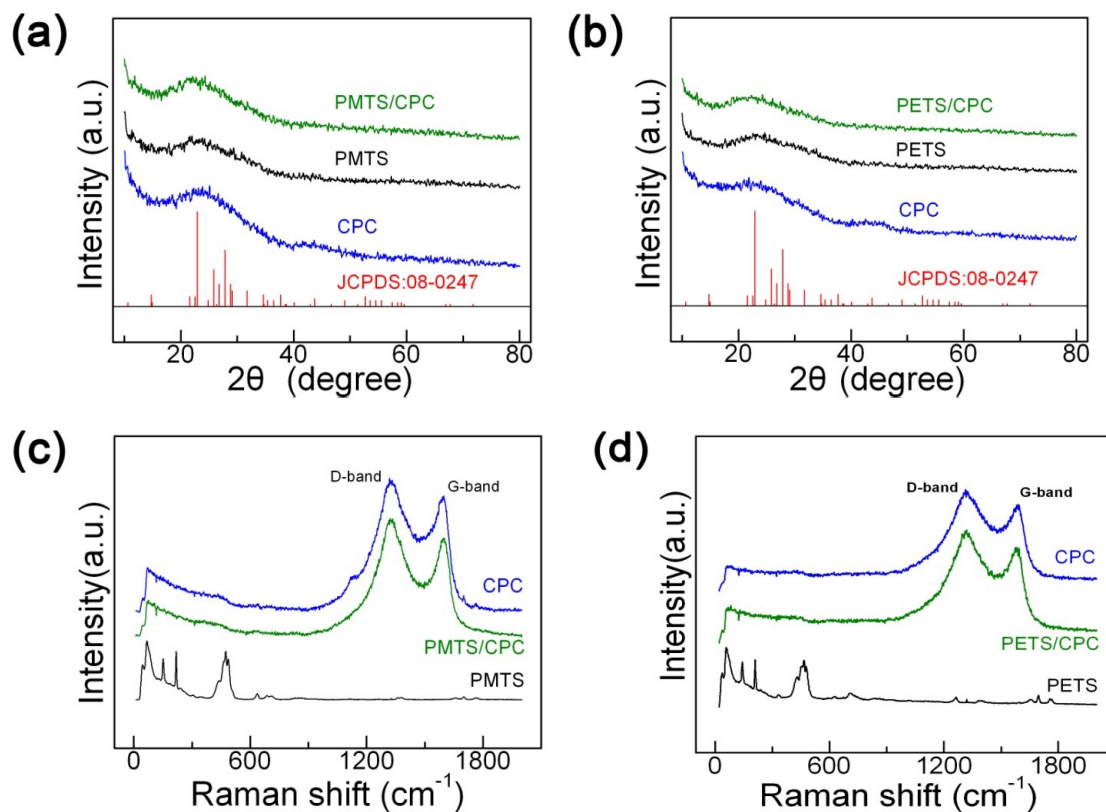


Fig. S3 (a, b) XRD patterns and (c, d) Raman spectra of pristine CPC, as-synthesized copolymer PMTS or PETS and composite PMTS/CPC or PETS/CPC.

XRD patterns and Raman spectra of composites PMTS/CPC and PETS/CPC only reveal the typical characteristics of a partially graphitized carbon, indicating the “homogeneous” distribution of polymer PMTS (or PETS) within the porous framework of CPC.

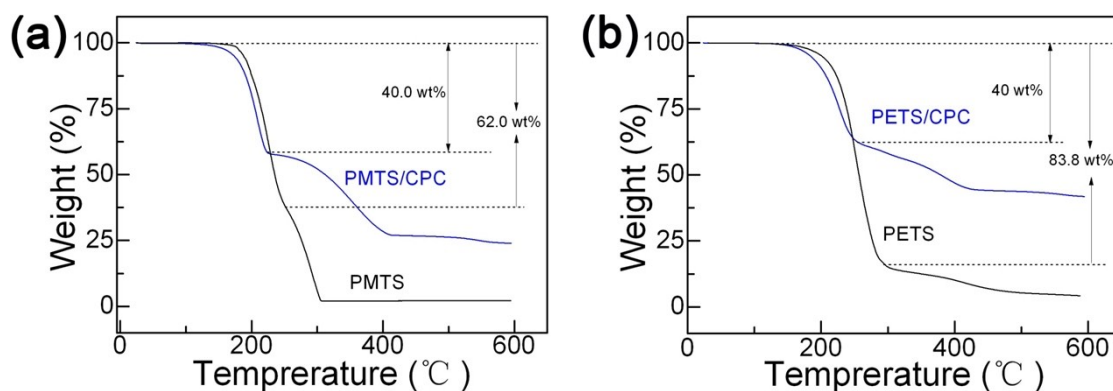


Fig. S4 Comparative TGA behaviors of as-synthesized copolymer and its corresponding composite: (a), PMTS and PMTS/CPC (5:2); (b), PETS and PETS/CPC (3:1).

Thermogravimetric behaviors of as-synthesized copolymers PMTS and PETS are in agreement with their corresponding data in literature reports, giving the “available” sulfur contents of 62.0 wt% and 83.8 wt%, respectively.^{8,13}

It should be emphasized that, as shown in Fig.S4, herein the two composites of PMTS/CPC and PETS/CPC were obtained at the copolymer:CPC weight ratio of 5:2 and 3:1 (w/w), respectively. Furthermore, according to the effective sulfur content of sulfur-containing polymers for Li-S battery cathodes reported in literatures,^{7,9} in context each effective sulfur content for the two composites of PMTS/CPC and PETS/CPC was determined by reproducible TGA measurements, giving a constant value of 40.0 wt%.

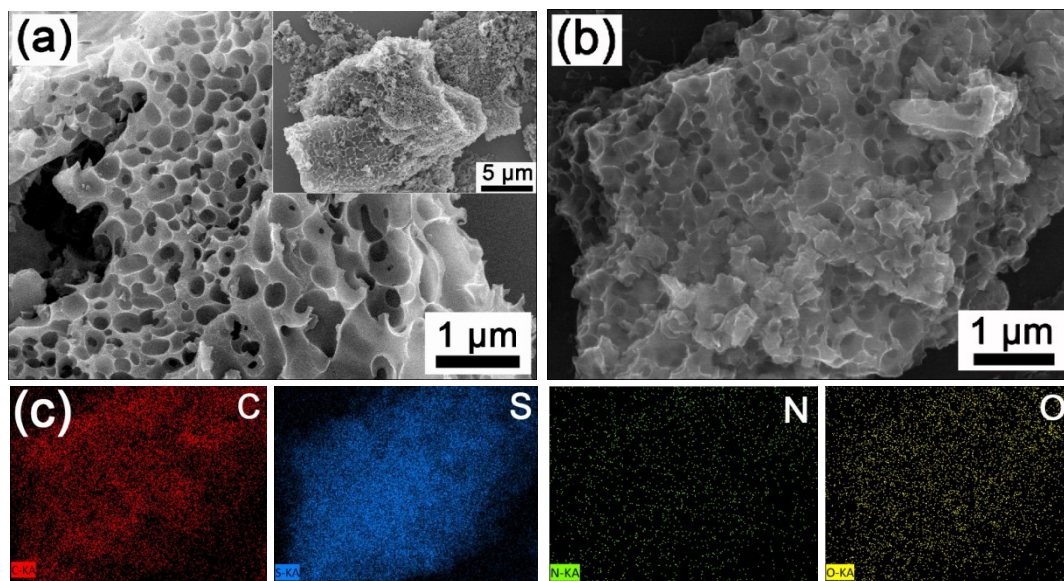


Fig. S5 (a) SEM images of pristine CPC, (b) SEM and (c) corresponding C, N, O and S elemental mapping images of PMTS/CPC composite.

Self-made framework of CPC belongs to a three-dimensional (3D) macro-/micro-porous structure (Fig.S5), and its electron-conductive nature mainly depends upon the clustering and orientation of sp^2 -hybridized carbon sites. As shown in Fig.S3, the actual graphitization of porous framework CPC could be explained by both the small sp^2 -carbon domains (e.g., < 5 nm) with a disordered arrangement and the large structural domains (e.g., > 1 μm) with a parallel arrangement.^{2,5,7,14-17}

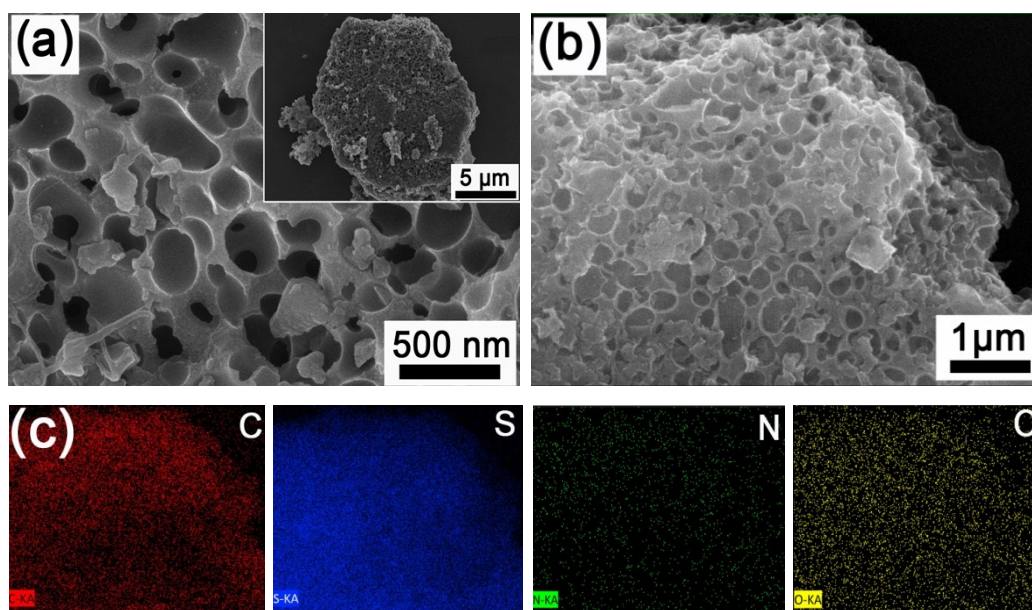


Fig. S6 (a) A high-resolution SEM image and its inserted overview of PETS/CPC composite. (b) SEM and (c) corresponding C, S, N and O elemental mapping images of PETS/CPC composite.

As shown in Fig.S5 or S6, the thoroughly mixing of PMTS or PETS with porous framework CPC guarantees the homogeneous distribution of elemental S or C therein.

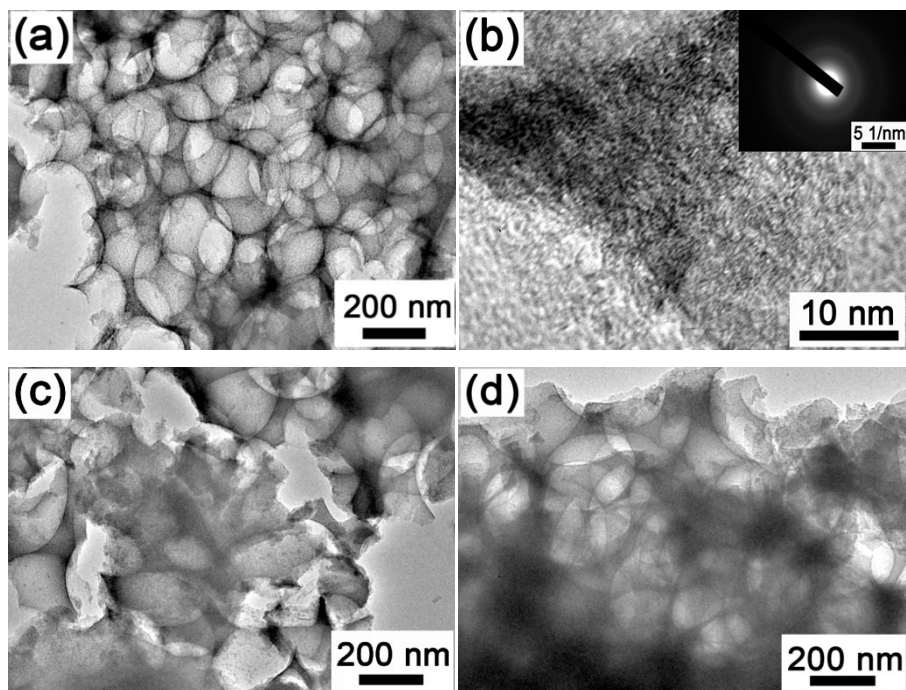


Fig. S7 (a) Low- and (b) high-resolution TEM images of pristine CPC, visually showing its macro- and/or microporous nature. (c, d) TEM images of PMTS/CPC and PETS/CPC composites.

The panel (b) of Fig. S7, as well as an inset of the corresponding electron diffraction pattern, indicates that the actual graphitization of framework CPC deals with both the small sp^2 -carbon domains (e.g., < 5 nm) with a disordered arrangement and the large structural domains (e.g., > 1 μm) with a parallel arrangement.

SEM pictures and the corresponding elemental mapping images of composite PETS/CPC (Fig.S6), together with the SEM and TEM observation of composite PMTS/CPC (Fig. S5, S7), indicate that the slightly solvent-stretching backbones of copolymeric PMTS or PETS can be “encapsulated” into the inner voids of framework CPC.

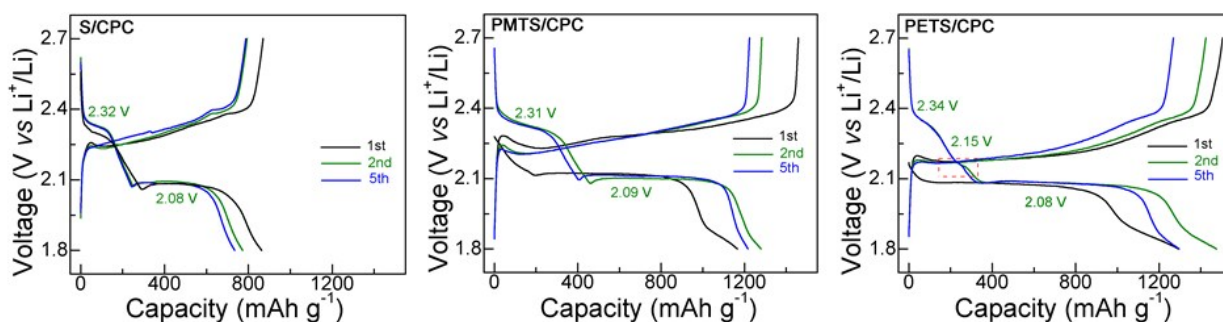


Fig. S8 Voltage profiles of S/CPC, PMTS/CPC and PETS/CPC composite electrodes operated at a current density of 0.2 C (1 C = 1675 mAh g⁻¹) within the voltage range of 1.8 - 2.7 V vs. Li⁺/Li.

Insofar as the 2nd discharge curve of each composite cathode is concerned, composites S/CPC and PMTS/CPC display two discharge plateaus at the first/second voltages of 2.32/2.08 and 2.31/2.09 V, respectively, whereas composite PETS/CPC interestingly presents three discharge plateaus at the first/second/third voltages of 2.34/2.15/2.08 V. These voltage profiles of composite cathodes S/CPC, PMTS/CPC and PETS/CPC coincide well with their CV behaviors (Fig. 2a-c) correspondingly.

Because the second discharge-voltage platform of PETS/CPC is too small to be negligible or may be integrated into the first discharge-voltage platform, the shape of the discharge curves of composite PETS/CPC is similar to that of PMTS/CPC or S/CPC.

As for the lithiation and PETS, the modified Li₂S₆-like intermediate is Li₂S₄CH₂CH₂ in chemical formula, while the chemical formula of Li₂S₄-like polysulfide is Li₂S₂CH₂CH₂. According to the experimental design and assumption listed in context, herein the Li₂S₄-like polysulfide of Li₂S₂CH₂CH₂ is electrochemically stable or cannot be further lithiated to produce Li₂S₃-like intermediate. That is, herein the intermediate Li₂S₃ or the products Li₂S₂/Li₂S originate from the long-chain polysulfides (e.g., Li₂S₈-like form of Li₂S₆CH₂CH₂).

Therefore, the modification of an intermediate polysulfide (e.g., only the one modified Li₂S₄ of Li-S-CH₂CH₂-S-Li, PETS) may influence the capacity ratio. By estimation, herein the capacities from PETS to Li-S-CH₂CH₂-S-Li and from Li-S-CH₂CH₂-S-Li to Li-S-Li are 360 and 1113 mAh g⁻¹, the capacity ratio between PETS to Li-S-CH₂CH₂-S-Li and Li-S-CH₂CH₂-S-Li to Li-S-Li is 1:3.1.

References

- 1 M. R. Kalae, M. H. N. Famili and H. Mahdavi, *Macromol. Symp.*, 2009, **277**, 81-86.
- 2 M. R. Kalae, M. H. N. Famili, M. Dadgar, M. R. T. B. Olyai and A. Naderi, *Phosphorus, Sulfur, Silicon and the Relat. Elem.*, 2010, **185**, 588-594.
- 3 H. S. Nasrabadi, M. R. Kalae, M. Abdouss, M. Sheydaei and S. Mazinani, *J. Inorg. and Organomet. Polym. Mater.*, 2013, **23**, 950-957.
- 4 H. S. Nasrabadi, M. R. Kalae, S. Mazinani, M. Abdouss and N. Sedaghat, *Polym. Plast. Technol. Eng.*, 2014, **53**, 767-774.
- 5 H. Zhang, D. Jia, Z. Yang, F. Yu, Y. Su, D. Wang and Q. Shen, *Carbon*, 2017, **122**, 547-555.
- 6 D. Jia, Z. Yang, H. Zhang, F. Liu and Q. Shen, *J. Alloys Compd.*, 2018, **746**, 27-35.
- 7 B.-C. Yu, J.-W. Jung, K. Park and J. B. Goodenough, *Energy Environ. Sci.*, 2017, **10**, 86-90.
- 8 M. R. Kalae, M. H. N. Famili, H. Mahdavi and A. Naderi, *Polym. Sci. Ser. B*, 2010, **52**, 286-291.
- 9 S. Zeng, L. Li, L. Xie, D. Zhao, N. Zhou, N. Wang and S. Chen, *Carbon*, 2017, **122**, 106-113.
- 10 G. Kresse and J. Furthmüller, *Phys. Rev. B*, 1996, **54**, 11169-11186.
- 11 G. Kresse and J. Furthmüller, *Comput. Mater. Sci.*, 1996, **6**, 15-20.
- 12 S. Grimme, *J. Comput. Chem.* 2006, **27**, 1787-1799.
- 13 M.R. Kalae, M.H.N. Famili, M. Dadgar, M.R.T.B. A. Olyai, *Sulfur Silicon Relat. Elem.* 2010, **185**: 588-594.
- 14 X. Ji, K. T. Lee and L. F. Nazar, *Nat. Mater.*, 2009, **8**, 500-506.
- 15 M. Chen, S. Jiang, C. Huang, X. Wang, S. Cai, K. Xiang, Y. Zhang and J. Xue, *ChemSusChem*, 2017, **10**, 1803-1812.
- 16 S. Osswald, J. Chmiola and Y. Gogotsi, *Carbon*, 2012, **50**, 4880-4886.
- 17 M. Pawlyta, J.-N. Rouzaud and S. Duber, *Carbon*, 2015, **84**, 479-490.